Generation of complex concentration profiles by partial diffusive mixing in multi-stream laminar flow

Yao Zhou,[a] Yi Wang,*[b] Tamal Mukherjee[c] and Qiao Lin*[a]

Received 31st October 2008, Accepted 27th January 2009
First published as an Advance Article on the web 27th February 2009
DOI: 10.1039/b818485b

This paper proposes novel microfluidic concentration gradient generator (CGG) devices that are capable of constructing complex profiles of chemical concentrations by laterally combining the constituent profiles (*e.g.*, linear and bell-shaped) generated in simple Y- or ψ-shaped mixers. While the majority of currently existing CGG devices are based on complete mixing of chemical species, our design harnesses partial diffusive mixing in multi-stream laminar flow, and hence, features simple network structures and enhanced device reliability. An iterative simulation approach that incorporates our previous system-level models of CGG networks is developed to locate best-matched combinations of geometrical and operating parameters (*e.g.*, inlet flow rates and inlet sample concentrations) for the device design. Microfluidic CGG chips are fabricated and experimentally characterized using optimal layout and operating conditions selected by the design process. The experimental results not only serve as a benchmark for model verification but also establish the feasibility of concentration gradient generation based on partial mixing for a variety of microfluidic applications.

1. Introduction

Concentration gradients (or concentration arrays) of diffusible chemicals or stimulating samples are widely used in lab-on-a-chip applications involving cell biology (*e.g.*, chemotaxis[1,2]), biochemistry,[3] surface patterning and microfabrication.[4,5] Conventionally, pipette injection into fluidic channel,[6] sample diffusion through gel,[7] the Boyden chamber[8] or their variants[9,10] are used to release the sample and to investigate cell behavior subject to certain concentration gradients of the sample. However, these techniques are inefficient in providing spatially stable gradients of complex shapes due to the unbalanced chemical flux into and from the region of interest.[11] On the other hand, a technique to generate and maintain predictable complex concentration gradients over an extended period of time is strongly desired in practice, for example, to examine the correlation between the gradient and cell behavior, and quantitatively compare the significance of competing gradients of different samples.[11,12]

Desired concentration gradients can be effectively produced in microfluidic networks, where molecules diffuse between multiple streams of laminar flow.[11] Most commonly, the networks consist of several hierarchical stages of microchannels followed by a single output microchannel.[11,13,14] In each stage of the microchannels, sample or buffer streams from the preceding stage are split into a larger number of streams, which are then recombined for complete inter-stream mixing *via* sample diffusion (*i.e.*, uniform sample concentration across the entire stream[15,16]). This process is repeated through all microchannel stages; and flow streams from the last stage are combined into a single stream in the output channel to form desired sample concentration gradients. To enable efficient design of such complete-mixing based microfluidic concentration gradient generator (CGG) devices, simple algebraic models derived from the flow-electrical analogy have been proposed to capture the variations of sample concentrations within the network (except for the output microchannels).[11] This approach has been applied to design diverse concentration profiles, such as linear, parabolic, sawtooth, and hybrid profiles.[2,11,13] Recently, Campbell and Groisman[17] further improved the approach by generating a monotonic concentration profile of any given shape and reducing the number of splitting-recombining-mixing stages logarithmically.

While widely used, concentration gradient generation by complete-mixing often requires overly long microchannels linked in complex topology, which consume large chip area and are prone to leakage and clogging. In addition, this approach produces discontinuous (step-like), non-smooth[14] concentration profiles in the output channel that may be undesirable for some applications. These limitations can be effectively addressed by a gradient generation approach that exploits partial mixing and multi-stream laminar flow configuration in the microfluidic network, leading to simplified network topologies. Along these lines, Holden *et al.*[18] reported a Y-shape laminar microfluidic diffusion diluter (mDD) that utilized side-by-side partial-mixing of samples to generate transverse concentration gradients. Walker *et al.*[19] employed a cross-mixing microfluidic device to produce a bell-shaped concentration profile of a virus, which was used to study cell infections in microscale environments. These devices, however, are limited to the generation of simple concentration profiles. Indeed, studies on applying the partial-mixing principle to create complex concentration profiles are

[a]*Department of Mechanical Engineering, Columbia University, New York, 10027, USA. E-mail: qlin@columbia.edu; Tel: +01 212-854-1906*
[b]*CFD Research Corporation, Huntsville, Alabama, 35805, USA. E-mail: yxw@cfdrc.com; Tel: +01 256-327-0678*
[c]*Department of Electrical and Computer Engineering, Carnegie Mellon University, Pennsylvania, 15213, USA*

scarce. The primary reason might be that the multiphysics (in particular, sample transport after stream combination) involved in partial mixing is much more complicated than in the complete mixing case.[15,16] Therefore, efficient transport models and robust design algorithms that are experimentally validated are strongly desired to guide the design of partial mixing-based CGGs.

To address these critical needs, this paper presents novel microfluidic CGG devices that construct complex-shaped sample/chemical concentration profiles by juxtaposing constituent profiles (*e.g.*, linear and bell-shaped) resulting from the partial mixing of samples in simple Y- or ψ-shaped mixers. To enable efficient design of the CGGs, an iterative simulation-based method is proposed, in which the system-level model representation of each candidate design (as we recently reported[16]) is successively evaluated to locate the optimal combination of the governing parameters. The optimal CGG layout obtained from the iterative process is then translated into a fabricated microchip, which is thoroughly characterized by experiments. Generation of complex concentration gradients (such as sawtooth-shaped and double bell-shaped profiles) that previously has been allowed only by the complete mixing-based methods is successfully demonstrated. This substantiates the capability of partial mixing-based CGGs for various lab-on-a-chip applications. The experimental results of the gradient generation show excellent agreement with those at the design phase, and hence, convincingly verify our models and design approach.

Building on our previous modeling work,[16] the present study addresses the development of the design algorithm, its application to practical CGG design, demonstration of generating complex concentration profiles by partial mixing, as well as the experimental verification of the models. As a result, we establish a self-contained, automated platform for efficient, system-level design of CGGs (spanning both partial- and complete-mixing-based devices).

The paper is organized as follows. The principles of the partial mixing-based gradient generation and the modeling methodology (including component- and system-level models) are first introduced in Section 2. Section 3 elucidates the iterative simulation-based design approach, which is followed by a description of the microchip fabrication and experimental setup (Section 4). In Section 5, a variety of practically useful concentration gradients generated *via* partial mixing are demonstrated. The modeling and design results are validated against experimental data. The paper concludes with a summary in Section 6.

2. Principle and modeling methodology

In this section, we will first illustrate the principle of the partial mixing-based CGG devices and then briefly describe the component models and system-level representations that will be used in a simulation-based design algorithm.

2.1 Partial mixing-based concentration gradient generation

Consider a Y-shaped mixer (Fig. 1a) and a ψ-shaped mixer (Fig. 1b), which comprise a junction (Y-shaped or ψ-shaped) and several microchannels connected to the junction. Given the microscale dimensions of the channel cross-section and the practically relevant flow rates, the Reynolds number of the flow is small and the molecular diffusion within laminar flow is the dominant mechanism for sample mixing between streams. In the Y-shaped mixer, the sample and buffer solvent merge at the junction and then mix with each other in the downstream mixing channel. The extent of sample mixing determines the shape of the resulting concentration profiles. For example, immediately after the junction, an abrupt step-shaped profile forms due to the negligible transverse diffusion. The transverse location of the discontinuity is determined by sample and buffer flow rates through both branch channels. The concentration profile evolves into a more smooth distribution as the sample migrates downstream. At the end of the channel, an approximately linear concentration profile is obtained, which exhibits good linearity in the central portion of the channel width. The gradient is modestly nonlinear at both sidewalls due to their impermeability to sample transport. Similarly, a sample stream sandwiched between two pure buffer streams can be introduced into a mixing channel (Fig. 1b). Immediately after the ψ-shaped junction, a Dirac delta function-like concentration profile forms because of a lack of sample mixing therein. Inter-stream diffusion in the downstream mixing channel smears out the abrupt gradient and produces a bell-shaped profile, which is commonly employed to investigate chemotaxis.[2] By selecting proper channel dimensions, flow rates and detection spots, desired height, width and transverse position of the bell shape can be obtained.

It is straightforward to conceive that by juxtaposing these constituent profiles laterally, temporally and spatially stable gradients of more complex shapes can be achieved. For example, a sawtooth-shaped concentration profile (including three linear segments) can be created by merging the approximately linear profiles emerging from three Y-shaped mixers. The associated network topology is depicted in Fig. 1c, which shows that the Y-shaped mixers are placed in parallel on a microchip, and their exits converge at a ψ-shaped junction. The sawtooth profile is then detected at the downstream output channel. As the constituent profiles are independent of each other, their shape characteristics (*e.g.*, width, slope, peak and mean concentration values) can be individually manipulated by judicious choice of branch flow rates, channel sizes, and flow ratios.

2.2 Component models

The microfluidic CGG device can be represented by a set of elementary components, including microchannels (straight or curved), Y- and ψ-shaped junctions (Fig. 2), and reservoirs. In a microchannel (Fig. 2a), sample and buffer streams flow side by side, and mix with each other by molecular diffusion in laminar flow (note that a channel containing only sample or buffer can be treated as a special case). A Y-shaped junction has two inlets, labeled as "L" and "R", and one outlet as "Out" (Fig. 2b). Sample and/or buffer streams enter the junction *via* the inlets and exit from the outlet as a single combined stream. Similarly, a ψ-shaped microchannel junction possesses three inlets, which are labeled as "L", "C", and "R", and one outlet as "Out" (Fig. 2c). Accordingly, three streams of sample and/or buffer solutions are concurrently introduced into the junction. Note that while not

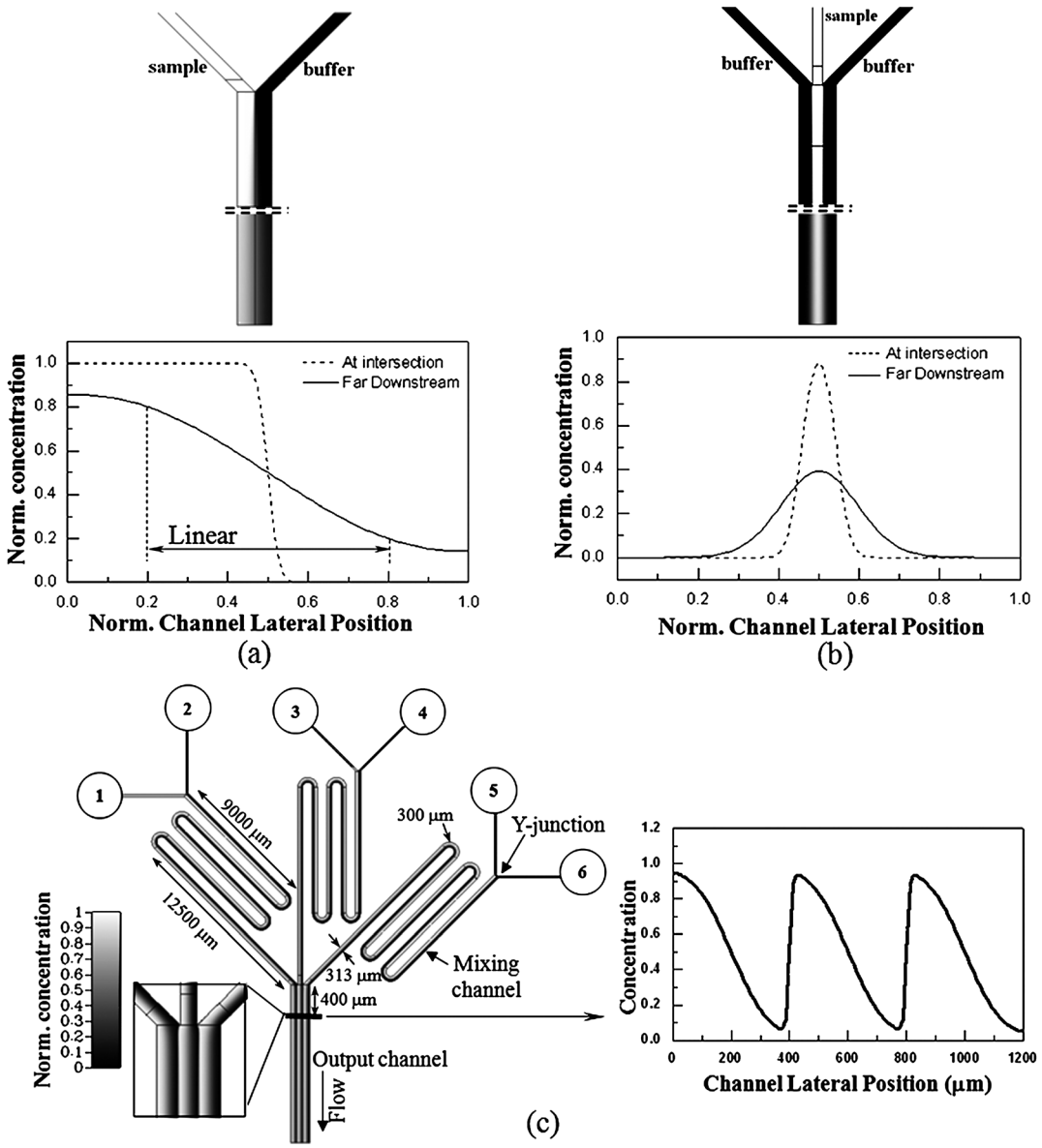

Fig. 1 Principle of CGGs based on partial mixing of samples. Constituent mixers: (a) a Y-shaped mixer and the generated concentration profile, and (b) a ψ-shaped mixer and the generated concentration profile. (c) a CGG, which consists of three Y-shaped mixers placed in parallel on a microchip, generates a sawtooth-shaped profile including three constituent linear profiles.

discussed here, junctions with four or more inlets could be used to combine more streams if desired.

As a complex microfluidic network can be decomposed into a collection of standardized components, a system-level modeling and simulation methodology will be utilized for CGG modeling in this paper. That is, models for individual components will be developed, which are then linked to construct a system-level model for the entire microfluidic network representation. Details of the component models are given elsewhere.[16] Here, to make this paper self-contained, we recapitulate the key elements of these models. Essentially, the objective of component modeling is to determine the functional relationship between the inlets and outlet in terms of fluidic pressure (p), flow rate (q), and sample concentration (c). To obtain the model in analytical form, we make the following assumptions. First, the length of the channel is much greater than its width and depth. Second, in practical applications, the mixing channel has a flat cross section, *i.e.*, the width is much larger than the depth. Third, a mixing channel can be either straight or curved in shape (*e.g.*, serpentine in Fig. 1c), in which case the effects of longitudinal curvature on the laminar flow and sample diffusion are negligible. Finally, the flow field is steady-state. The implications and justification of these assumptions are discussed in Ref. 16.

2.2.1 Microchannel model. By solving the flow momentum equation and convection-diffusion equation along with the assumptions above, at the inlet and outlet of a microchannel, the pressure (p), flow rate (q), and Fourier coefficients (d_n) (defined below) are given by[16,20]

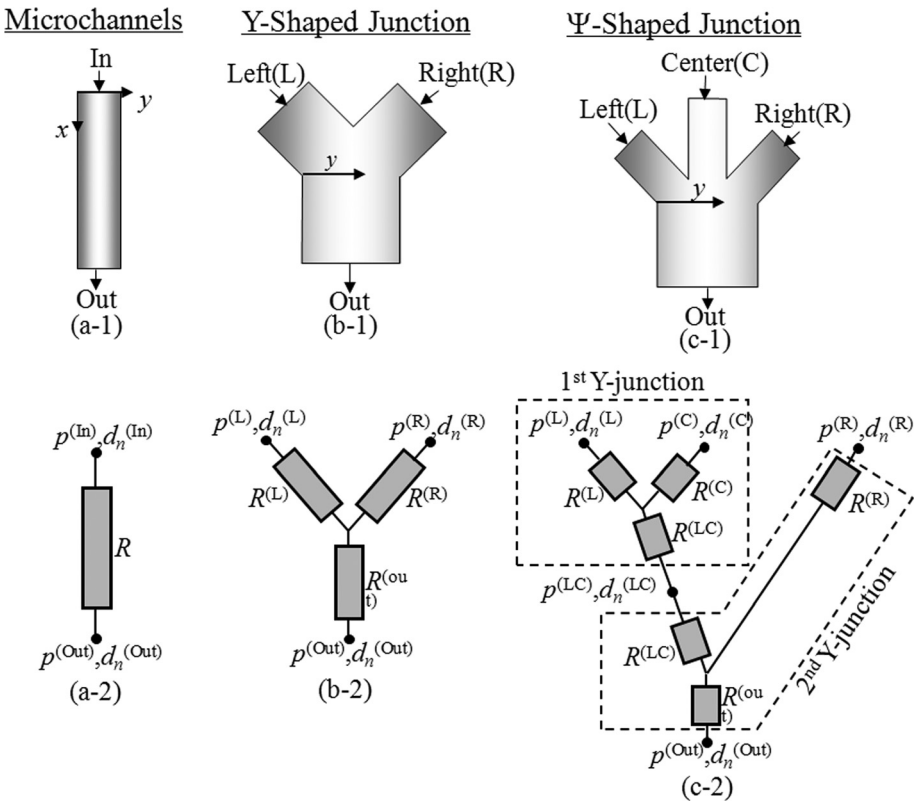

Fig. 2 Elementary components and models for concentration gradient generation: (a-1) a microchannel (straight or curved), (a-2) the model for the microchannel; (b-1) a Y-shaped junction, (b-2) the model for the Y-shaped junction; (c-1) a ψ-shaped junction, and (c-2) the model for the ψ-shaped junction. The ψ-shaped junction is modeled as a serial connection of two Y-shaped junctions. Here R denotes the flow resistance of the component.

$$p^{(\mathrm{out})} = p^{(\mathrm{in})} + Rq,\ R = \frac{12\beta l\varpi}{w^4\left[1 - \frac{192\beta}{\pi^5}\sum_{i=1,3,5\ldots}^{\infty}\frac{\tanh(i\pi/2\beta)}{i^5}\right]} \quad (1)$$

and

$$d_n^{(\mathrm{out})} = d_n^{(\mathrm{in})} e^{-(n\pi)^2\tau} \quad (2)$$

where subscript "in" and "out" represent the quantities at the inlet and outlet of the channel, q is the volumetric flow rate through the channel, R is the channel's flow resistance, β is the channel's aspect ratio, defined as the ratio of channel width w to the depth h, l is the channel length, ϖ is the dynamic viscosity of the solution. Also $\tau = lD/(Uw^2)$ is the dimensionless residence time of the sample in the channel, where U is the average flow velocity across the channel's cross-section. The concentration profile of the sample at any location in the network (including inlets and outlets) can be written by $c(\eta) = \Sigma_{n=0}^{\infty} d_n \cos(n\pi\eta)$, where d_n is the Fourier coefficients ($n = 0, 1, 2,\ldots$), y and $\eta = y/w$ are, respectively, the dimensional and dimensionless transverse coordinate (Fig. 2). Eqs. (1) and (2) also apply to a curved microchannel turn having a rectangular cross section (Fig. 1c), with the centerline arc length given by $l = r_c\theta$, where r_c and θ are, respectively, the mean radius and included angle of the turn.

2.2.2 Y-Shaped junction. In a Y-shaped junction two incoming streams with certain sample concentration profiles are juxtaposed and emerge as a single combined stream (Fig. 2b). As the flow path lengths of the Y-junction are negligible compared with those of the channels, such an element can be assumed to have zero physical size. Thus, the pressures and the Fourier coefficients of the sample concentration at the inlets and outlet are related by

$$p^{(\mathrm{L})} = p^{(\mathrm{R})} = p^{(\mathrm{out})},\ R^{(\mathrm{L})} = R^{(\mathrm{R})} = R^{(\mathrm{out})} = 0 \quad (3)$$

and

$$d_n^{(out)} = \begin{cases} d_0^{(L)}s + d_0^{(R)}(1-s), & \text{if } n=0 \\ s\sum_{m=0}^{\infty,\,\text{if } m\neq ns} d_m^{(L)}\frac{f_1\sin(f_2)+f_2\sin(f_1)}{f_1 f_2} + s\sum_{m=0}^{\infty,\,\text{if } m=ns} d_m^{(L)} + (1-s)\sum_{m=0}^{\infty,\,\text{if } m=n(1-s)}(-1)^{n-m}d_m^{(R)} & \\ \quad + 2(-1)^n(1-s)\sum_{m=0}^{\infty,\,\text{if } m\neq n(1-s)} d_m^{(R)}\left(\frac{\cos(F_2/2)\sin(F_1/2)}{F_1} + \frac{\cos(F_1/2)\sin(F_2/2)}{F_2}\right), & \text{if } n\geq 1 \end{cases} \quad (4)$$

where "L", "R", and "out", respectively, denote the quantities at the left inlet, right inlet and outlet; $s = q^{(\mathrm{L})}/(q^{(\mathrm{L})} + q^{(\mathrm{R})})$ is the flow ratio at the junction, *i.e.*, the normalized flow rate of the left-branch stream, and gives the normalized position of the interface between the incoming streams. Here, $f_1 = (m - ns)\pi$, $f_2 = (m + ns)\pi$, $F_1 = (m + n - ns)\pi$ and $F_2 = (m - n + ns)\pi$.

2.2.3 ψ-Shaped junction. To develop a separate model for the ψ-shaped junction is unnecessary, as the ψ-shaped junction can be constructed as a serial connection of two Y-shaped junctions (Fig. 2c). Likewise, the pressures at all inlets and outlet are identical due to zero physical size of the junction:

$$p^{(\mathrm{L})} = p^{(\mathrm{C})} = p^{(\mathrm{LC})} = p^{(\mathrm{R})} = p^{(\mathrm{out})},$$
$$R^{(\mathrm{L})} = R^{(\mathrm{C})} = R^{(\mathrm{LC})} = R^{(\mathrm{R})} = R^{(\mathrm{out})} = 0 \quad (5)$$

As to the Fourier coefficients, the output of the first Y-shaped junction is used as the input to the left inlet of the second Y-shaped junction. Specifically, given the Fourier coefficients of the sample concentration at the left $d_n^{(L)}$ and the center inlets $d_n^{(C)}$, Eq. (4) is used to calculate the Fourier coefficients $d_n^{(LC)}$ at the outlet of the first Y-shaped junction. $d_n^{(LC)}$and that at the right inlet $d_n^{(R)}$ are then supplied as the inputs to Eq. (4) of the second Y-shaped junction to calculate the overall output coefficient $d_n^{(out)}$of the ψ-shaped junction.

2.3 System-level models

The design process requires the use of a system-level model representing the whole CGG device of the candidate design for performance evaluation. This is accomplished by linking the component models described above according to the device topology (see Ref. 16 for a more detailed discussion of model integration).

The use of the system model to evaluate the candidate design involves computing both fluidic parameters including pressure (p), flow rates (q), and the Fourier coefficients (d_n) of the concentration profile along the channel width for all components in the network. Parameters between two neighboring components are set equal, *i.e.*, $(P^{(i)})^{j+1} = (P^{(out)})^j$ and $\{d_n^{(i)}\}^{j+1} = \{d_n^{(out)}\}^j$ because of continuity requirements, where the index i has values "in", "L", or "R", respectively, to represent the component's inlet, left, or right inlets, j denotes the j^{th} component in the network and its immediately downstream component is numbered $j + 1$.

The specific computational procedure is as follows.[16] Given a system topology, component geometries and volumetric flow rates (or equivalently applied pressures) at reservoirs, the flow rate through each component in the entire CGG network is first computed using Eqs. (1), (3), and (5) along with Kirchhoff's law. The flow rate (q), average flow velocity U, and the direction of the stream within each component, as well as the flow ratio s at the junctions are then explicitly calculated. With these results and user-input sample diffusivity D, Fourier coefficients of sample concentrations $\{d_n^{(out)}\}^j$at the outlet of component j are determined from the corresponding values at the component inlets, and then assigned as an input to the inlet of its succeeding component $j + 1$, for which the sample concentration Fourier coefficients $\{d_n^{(out)}\}^{j+1}$ can be computed in a similar manner. This procedure starts from the most-upstream sample reservoirs, and continues until the most-downstream component (waste reservoir). Once the Fourier coefficients at each component are available, the concentration profile within the entire network (including that at the detector location) can be reconstructed with $c(\eta) = \Sigma_{n=0}^{\infty} d_n \cos(n\pi\eta)$.

Finally, it should be noted that all the component models and system-level modeling approach could be extended to devices that use electrokinetically driven flow.[21] In this case, the assumption of flat channel cross sections can be relaxed.[16]

3. Iterative simulation-based CGG design

In practice, it is often necessary to design a device that generates a user-prescribed concentration profile. This can be accomplished using an iterative simulation process, in which a set of candidate designs spanning a user-specified parameter space is successively evaluated to identify the best choice. To facilitate the formulation of this process, a profile discrepancy index, $E_{\{d,p\}}$, is defined to characterize the discrepancy between the prescribed profile c_p and the profile produced by the individual candidate design c_d in the iterative process:

$$E_{\{d,p\}} = \frac{\int_{\eta_1}^{\eta_2} \left| c_d(\eta) - c_p(\eta) \right| \cdot d\eta}{\int_{\eta_1}^{\eta_2} c_p(\eta) \cdot d\eta} \quad (6)$$

where η_1 and η_2 ($0 \le \eta_1 < \eta_2 \le 1$) represents the transverse region of interest in which the concentration profiles are evaluated. $E_{\{d,p\}}$ falls in the interval [0, 1] and a small value of $E_{\{d,p\}}$ indicates good agreement between the two profiles $c_d(\eta)$ and $c_p(\eta)$.

As shown in Fig. 3, the process begins with the choice of a suitable topology of the device according to the user-prescribed concentration profile (*e.g.*, linear, bell-shaped, or sawtooth-shaped). Then proper component models are selected and linked to provide the system-level representation of the device. The behavior of individual candidate CGG design is governed by a set of parameters including the dimensions of each component (*e.g.*, the length l, width w and height h of the channels), properties (*e.g.*, sample diffusivity D), and operating conditions (*e.g.*, sample concentrations c and flow rates q at the inlet reservoirs, and the detector location l_d). In general, all these parameters can be treated as design variables and be determined from the iterative process. However, in practice, it may be desirable to use a single device to produce multiple concentration gradient profiles. As shown in Fig. 3, we focus on this important scenario by selecting operating parameters as design variables for fixed

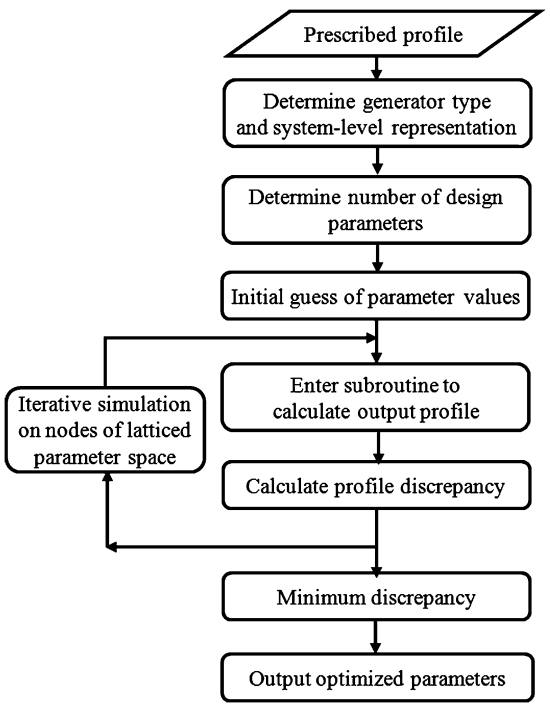

Fig. 3 A flow chart illustrating the iterative simulation-based design approach.

device geometry. Given initial guess values of design variables, the modeling subroutine assembles all the necessary information and calculates the output concentration profile c_d as well as its discrepancy from c_p at the position of detection. This step progresses iteratively at the nodes of the latticed user-defined parameter space to find out the best parameter combination yielding minimal $E_{\{d,\ p\}}$. This iterative procedure later can be improved in terms of automation and convergence speed by incorporating an appropriate optimization engine. It should be noted that if needed, the device dimensions also could be added as design variables in the above process. In addition, this design methodology also applies to electrokinetic CGG devices, in which the electrical potential at the reservoirs rather than the flow rate can be chosen as a design variable.

4. Microfabrication and experimental setup

Microfluidic CGG chips are fabricated according to the optimal design layout obtained from the aforementioned procedure. The chip consists of a sheet of poly(dimethylsiloxane) (PDMS) bonded to a glass substrate. The microfluidic features are fabricated in the PDMS sheet using soft lithography techniques. The fabrication process begins with spin-coating and patterning a 60-μm layer of SU-8 2050 photoresist (MicroChem, MA) on a silicon wafer, which upon curing at 95 °C for 7 min on a hotplate forms a master defining the negative of desired microfluidic features. Next, a PDMS prepolymer (Sylgard 184, Dow Corning, MI) is cast against the master and cured at 70 °C for 45 min, also on the hotplate. The resulting PDMS sheet is then peeled off from the master, cut into properly sized pieces, and punched with inlet and outlet holes. The PDMS is bonded to a glass slide (Corning, NY) after being placed for 5 minutes in a UV ozone cleaner (Model T10X10/OES, UVOCS, PA). Tygon tubes (Saint-Gobain Performance Plastics, OH) are inserted into the inlet and outlet holes in the PDMS and affixed with Epoxy (ITW Performance Polymers, FL). Fig. 4 illustrates the fabricated CGG micro-device (with ink solution filled in the channels), and the insets show the generation of concentration gradient using fluorescent solution.

A 10 μM stock solution of Alexa 488 (Sigma-Aldrich, MO) is prepared in phosphate buffer saline (PBS). Diluted concentrations are obtained by adding aliquots of the stock solution to PBS. In the experiments, fluorescent solutions and PBS buffer, at Alexa concentrations and the flow rates resulting from the iterative design process, are driven into the CGG devices using syringe pumps (KD230P, KD Scientific, MA). For generation of double bell-shaped profile (see below), an additional syringe pump (NE-1000, New Era Pump Systems, NY) is used. Fluorescent images are taken with an inverted epi-fluorescence microscope (Diaphot 300, Nikon Instruments, NY) and recorded by a CCD camera (Model 190 CU, Micrometrics, NH). Fluorescent intensity profiles across channel width are extracted from the images using ImageJ (available free online at http://rsb.info.nih.gov/ij/). For convenience of data presentation, all fluorescence intensity values are normalized against that of the stock solution.

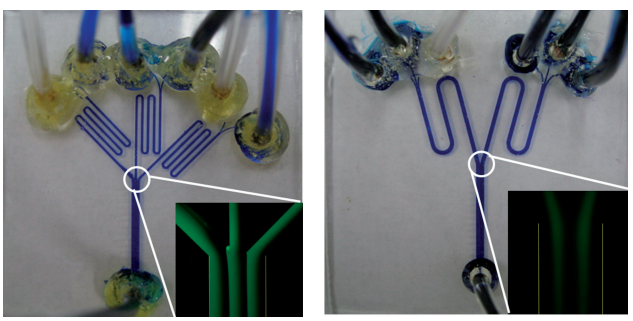

Fig. 4 The CGG device fabricated by the soft lithography technique. (a) CGG for sawtooth-shaped profile, and (b) CGG for double bell-shaped profile. The insets show the generation of concentration gradient using fluorescent solution.

5. Results and discussion

This section presents several microfluidic CGGs that are designed, fabricated and tested as described above. We will consider a set of practically important concentration gradients, including linear, bell-shaped, sawtooth-shaped, and double bell-shaped profiles. The concentration profiles measured in the experiments are then compared to the user-prescribed profiles and those from the design phase to validate the system model, and more importantly, to substantiate the feasibility of generating complex concentration gradients using the partial mixing approach.

In the discussion below, we will need to assess the discrepancies of an experimentally obtained concentration profile, $c_e(\eta)$ as compared with the corresponding user-prescribed concentration profile, $c_p(\eta)$, and design-generated profile, $c_d(\eta)$. We use indices that are defined in a similar fashion to Eq. (6) to characterize these discrepancies, with the subscripts $\{d, p\}$ respectively replaced with $\{e, p\}$ and $\{d, e\}$ to represent comparisons between the experimental and prescribed profiles, and between the design-generated and experimental profiles. Note again that $0 \leq \eta_1 < \eta_2 \leq 1$ in Eq. (6).

5.1 Linear profiles

We first demonstrate the design and experimental results of CGG devices to produce a prescribed linear concentration profile, which is mathematically represented by

$$c = a + b\eta \tag{7}$$

where a and b are constants. As discussed in Section 2.1, this profile can be generated with a Y-shaped mixer (see Fig. 1a). The device dimensions and normalized sample concentrations at the inlet reservoirs ($c_L = 1$ and $c_R = 0$ at the left- and right-inlets) are fixed, while the iterative design process is carried out to determine the flow rates q_L and q_R yielding sample concentration profile closest to the prescribed one. Here, consider two prescribed linear concentration profiles given by $\{a, b\}^{(I)} = \{1.5, 2\}$ (called Linear Profile I), and $\{a, b\}^{(II)} = \{2.5, 4\}$ (called Linear Profile II). The length and width of both branch channels are 8000 μm and 212 μm, and those of the output channel are 10000 μm and 600 μm. The detector is located at 10 mm downstream of the Y-shaped junction. Given these device dimensions, the proper flow rates yielded by the iterative simulation are: $\{q_L,$

$q_R\}^{(I)} = \{0.722, 0.722\}$ μl/min and $\{q_L, q_R\}^{(II)} = \{3.445, 3.445\}$ μl/min. The concentration profiles from the design and experiments are compared to the prescribed ones in Fig. 5a. Good agreement is found in the central region over the microchannel width. Specifically, at the detector position, the discrepancy between the design profile and prescribed profile over the central portion ($0.4 \leq \eta \leq 0.6$) is characterized by $E_{\{d,p\}} = 0.2$ % (Linear Profile I) and 1.9 % (Linear Profile II), and that between the experimental and prescribed profiles is $E_{\{e,p\}} = 1$ % (Linear Profile I) and 11.1 % (Linear Profile II). The deviation of design and experimental profiles from the prescribed profiles is appreciable near the channel sidewalls ($0 \leq \eta < 0.4$ and $0.6 < \eta \leq 1$) and can be attributed to impermeability of the walls to sample transport. However, this generally would not affect practical applications (*e.g.* cell chemotaxis), as the observation of biological behavior (*e.g.*, cell response) is extracted typically only in the central linear region for analysis. It should also be pointed out that the bending of the linear profile at the sidewalls is present even for complete mixing-based gradient generation as the inter-stream diffusion is typically needed for profile smoothing;[14] while the use of a large number of branches markedly alleviates such side effects.[11]

Fig. 5a also reveals that larger flow rates, accompanied by a narrower central linear region, are required to produce the concentration profile of a larger gradient ($dc/d\eta = 4$). The width of the central linear region is determined by the sample transverse diffusion length (w_d), and accordingly, the longitudinal sample residence time (t), which are correlated by $w_d = (2Dt)^{1/2}$. At higher flow rates, the longitudinal sample residence time and transverse diffusion length are both shorter (given a fixed detector location), leading to narrower central linear region.

To experimentally verify our system-level models,[16] we further compare the experimental and design results. Note that the comparison is carried out over the entire channel width ($0 \leq \eta \leq 1$), as the models are able to capture the diffusion behavior at the sidewalls. Excellent agreement is observed, with relative errors of $E_{\{d,e\}} = 2.6\%$ (Linear Profile I) and 4.3% (Linear Profile II). The discrepancy can be attributed to both approximations in the models and errors in fluorescence experiments. In the model, a large channel width-to-depth ratio is assumed,[16] which in turn leads to the assumption of a uniform cross-sectional velocity. This essentially neglects velocity boundary effects at the channel walls, and results in the near-wall discrepancies between the profiles. In experiments, errors in the actual flow rates of the syringe pumps would result in a small lateral shift in the measured concentration profile with respect to the design profile, and the shift is exacerbated for steeper profiles, as is evident from Fig. 5a.

5.2 Bell-shaped profiles

A symmetric bell-shaped profile along the channel width can be mathematically described in terms of two error functions,

$$c = \{\mathrm{erf}[a(\eta - b)] - \mathrm{erf}[a(\eta - 1 + b)]\}/2 \quad (8)$$

where a and b are constants, respectively, determining the slope and position of the sigmoid sides of the bell shape profile. This profile can be produced by a CGG device consisting of a single ψ-shaped mixer (Fig. 1b). In the device design, we again hold device dimensions and inlet sample concentrations, and perform the iterative design to determine the flow rates of the sample and buffer solutions at the L-, C- and R-inlets (q_L, q_C and q_R). The device dimensions are as follows: the length and width of the three branch channels are 8000 μm and 156.72 μm, and those of the output channel are 10000 μm and 600 μm. Detection is made at the end of the output channel. Given the device dimensions and inlet concentrations, flow rates of $\{q_L, q_C, q_R\}^{(I)} = \{2.532, 0.844, 2.532\}$, $\{q_L, q_C, q_R\}^{(II)} = \{6.594, 2.198, 6.594\}$, and $\{q_L, q_C,$

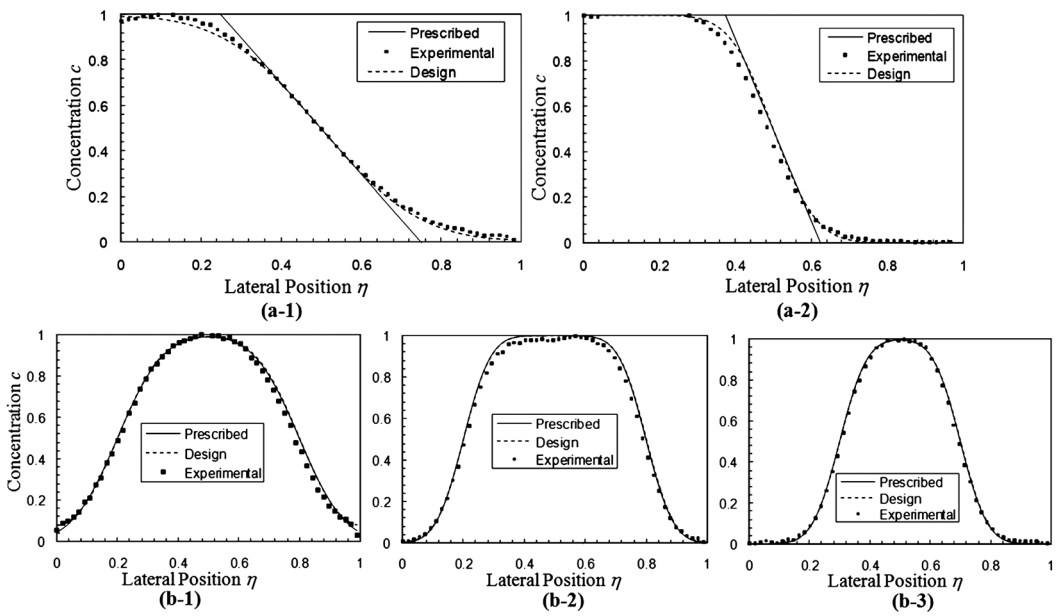

Fig. 5 Comparison of the prescribed, design, and experimental results of the constituent concentration profiles: (a-1) linear profile with $\{a, b\}^{(I)} = \{1.5, 2\}$ and (a-2) linear profile with $\{a, b\}^{(II)} = \{2.5, 4\}$; (b-1) bell-shaped profile with $\{a, b\}^{(I)} = \{6, 0.2\}$, (b-2) bell-shaped profile with $\{a, b\}^{(II)}.=.\{10, 0.2\}$, and (b-3) bell-shaped profile $\{a, b\}^{(III)}.=.\{10, 0.3\}$.

$q_R\}^{(III)} = \{3.295, 4.395, 3.295\}$ μl/min are obtained from the iterative design process to produce, respectively, three concentration profiles given by $\{a, b\}^{(I)} = \{6, 0.2\}$ (called Bell Profile I), $\{a, b\}^{(I)} = \{10, 0.2\}$ (Bell Profile II), and $\{a, b\}^{(III)} = \{10, 0.3\}$ (Bell Profile III). It shows that relative to Profile I, large flow rates are needed in Profile II to expedite the sample migration in the main microchannel for less diffusion, steeper side slopes, and more drastic gradient change (*i.e.*, larger values of $a = 10$). As the sigmoidal position parameter b increases, both sigmoid sides translate towards the channel centerline, shrinking the width of the plateau and the area under the curves. This can be achieved by reducing the ratio q_C/q_L (or q_C/q_R) to reduce the amount of sample entering the network. Further increase in b can result in a Gaussian or a Dirac δ profile without plateaus. The concentration profiles from the design and experiments are both compared to the prescribed profiles in Fig. 5b. They all agree well over the entire mixing channel width (in contrast to agreement found only in the central region for linear profiles). This is because the prescribed profiles expressed by error functions precisely capture the diffusion physics at the sidewalls and zero gradients therein. The discrepancy between the design and prescribed profiles for all the three cases are almost indistinguishable, characterized by $E_{\{d,p\}} = 1\%$ (Bell Profile I), 0.28% (Bell Profile II), and 0.39% (Bell Profile III) over the entire channel width. The relative errors between the experimental results and the prescribed profiles are found to be $E_{\{e,p\}} = 2.76\%$ (Bell Profile I), 3.56% (Bell Profile II), and 2.86% (Bell Profile III).

To examine the model accuracy, the design profiles obtained from model evaluation are also validated against the experimental results. Again the agreement is excellent, as indicated by relative errors of $E_{\{d,e\}} = 3\%$, 3.77%, and 2.98%, for Bell Profiles I, II and III, respectively.

5.3 Generation of sawtooth-shaped profiles

In this section, a CGG device is introduced to generate a sawtooth-shaped profile, which can be used, for example, for concurrent multiplex analysis or study of cell behavior subject to abrupt gradients. Consider N periodic constituent linear profiles lined up along the channel width, such that the i^{th} linear profile spans the transverse interval given by $(i-1)/N \le \eta \le i/N$ $(i = 1,2,\ldots,N)$. The overall profile can be mathematically represented by

$$c = a_i + b_i\eta \quad , \quad (i-1)/N \le \eta \le i/N \tag{9}$$

where a_i and b_i are constants, respectively determining the intercept (across the coordinate of normalized concentration) and slope of the constituent linear profiles.

We specifically focus on the case of three constituent linear profiles ($N = 3$). The CGG device consists of three Y-mixers, each generating one linear profile as shown in Fig. 1c. In order to produce a sharp sawtooth shape, the detection spot is chosen at 400 μm downstream from the Ψ-shaped junction that combines the Y-mixers. To demonstrate the feasibility of manipulating inlet concentrations to adjust concentration gradients, the device dimensions and flow rates are fixed in this example and the sample concentrations at the inlets are treated as design variables.

Given the device dimensions in Fig. 1c and a flow rate of 5 μl/min at each inlet, the iterative design procedure determines that inlet sample concentrations of $\{c_1, c_2, c_3, c_4, c_5, c_6\}^{(I)} = \{0.408, 0, 0.408, 0, 0.408, 0\}$ are required to generate a sawtooth-shaped profile with $\{a_1, b_1, a_2, b_2, a_3, b_3\}^{(I)} = \{0.5, -1.8, 1.1, -1.8, 1.7, -1.8\}$ (Sawtooth Profile I). The constraints $c_1 = c_3 = c_5$ and $c_2 = c_4 = c_6$ embedded in the concentration choices ensure the same slope and peak values of the three constituent linear profiles. Similarly, to achieve a sawtooth profile depicted by $\{a_1, b_1, a_2, b_2, a_3, b_3\}^{(II)} = \{1.3, -4.8, 1.1, -1.8, 0.57, -0.6\}$ (Sawtooth Profile II), inlet concentrations of $\{c_1, c_2, c_3, c_4, c_5, c_6\}^{(II)} = \{1, 0, 0.408, 0, 0.136, 0\}$ are needed. The constraints of the inlet concentrations $c_1 > c_3 > c_5$ and $c_1 - c_2 > c_3 - c_4 > c_5 - c_6$ render the peak values and slopes of the constituent linear profiles to decrease continually from the left to the right.

Similar to the single linear profile case, the concentration profiles from the design and experiments agree well with the prescribed ones in the central section of each constituent linear profile ($2/15 \le \eta \le 3/15$, $7/15 \le \eta \le 8/15$, and $12/15 \le \eta \le 13/15$ in Fig. 6). The total discrepancies summed over the three central portions are quantitated, for Sawtooth Profiles I and II, by $E_{\{d,p\}}^{(I)} = 2.1\%$, $E_{\{d,p\}}^{(II)} = 0.8\%$, $E_{\{e,p\}}^{(I)} = 7.2\%$, and $E_{\{e,p\}}^{(II)} = 10\%$. In addition to errors at the sidewalls, appreciable discrepancies are also observed at the interface between constituent linear profiles. This can be attributed to the inter-stream diffusion, which slightly smears out the linear gradient.

The experimental profiles are also compared to those obtained from iterative design for model verification. An agreement with relative errors of $E_{\{d,e\}}^{(I)} = 7.1\%$ (Sawtooth Profile I) and $E_{\{d,e\}}^{(II)}$

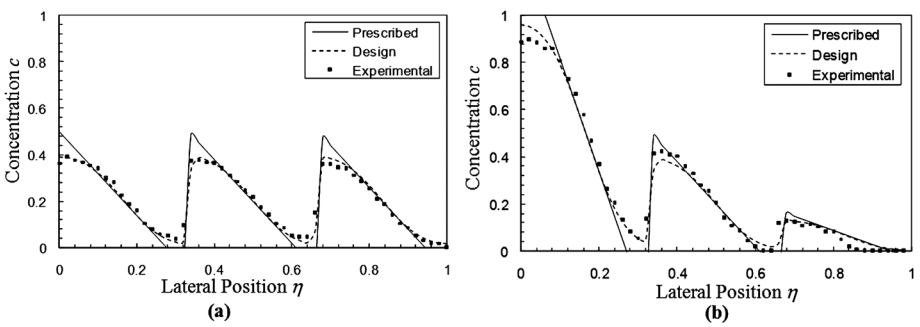

Fig. 6 Comparison of the prescribed, design, and experimental results of the sawtooth-shaped concentration profiles represented by (a) $\{a_1, b_1, a_2, b_2, a_3, b_3\}^{(I)} = \{0.5, -1.8, 1.1, -1.8, 1.7, -1.8\}$, and (b) $\{a_1, b_1, a_2, b_2, a_3, b_3\}^{(II)} = \{1.3, -4.8, 1.1, -1.8, 0.57, -0.6\}$.

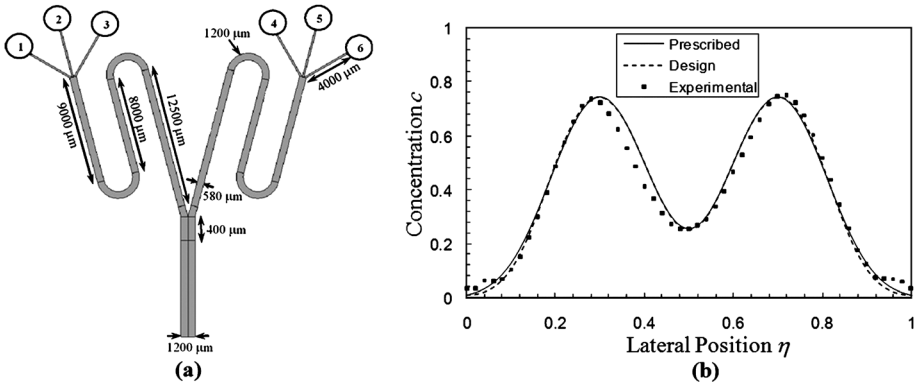

Fig. 7 A CGG device to produce a double bell-shaped concentration profile: (a) device layout and dimensions; and (b) comparison of the prescribed, design, and experimental results of the double bell-shaped concentration profiles, represented by $\{a, b, d\} = \{8, 0.2, 0.4\}$.

= 9.4% (Sawtooth Profile II) is observed over the entire channel width. Note again that since our models are able to describe the diffusion behavior accurately at the stream interfaces between the constituent linear profiles and at the sidewalls, the comparison is examined over the entire width. The most significant discrepancy occurs at the stream interfaces, where the concentration changes drastically, and can be attributed to the lateral profile shift arising from experimental errors in the actual flow control.

5.4 Double bell-shaped profiles

Our partial mixing-based CGG device is also capable of generating double bell-shaped concentration profile, which consists of two constituent bell-shaped profiles with partial overlap at the center and is similar to parabolic profiles generated with complete-mixing networks.[11] The profile is represented by

$$c(\eta) = \tfrac{1}{2}[erf(a(\eta - b)) - erf(a(\eta - d))] + \tfrac{1}{2}[erf(a(1 - \eta - b)) - erf(a(1 - \eta - d))] \quad (10)$$

This profile can be generated by a CGG network consisting of two ψ-shaped mixers juxtaposed side by side as shown in Fig. 7a. The channel dimensions are held unchanged during the design process, while the inlet flow rates and inlet concentrations are both treated as design variables. The profile is detected at 400 μm downstream from the Y-junction where two branch ψ mixers meet. Given a prescribed profile expressed by $\{a, b, d\} = \{8, 0.2, 0.4\}$, the iterative design process yields the proper flow rates and concentrations: $\{q_1, q_2, q_3, q_4, q_5, q_6\} = \{3.93, 4.78, 2.02, 2.02, 4.78, 3.93\}$ μl/min and $\{c_1, c_2, c_3, c_4, c_5, c_6\} = \{0, 0.84, 0.11, 0.11, 0.84, 0\}$.

The concentration profiles resulting from the design and experiments agree with the prescribed profile over the entire channel width (Fig. 7b), yielding relative errors of $E_{\{d,p\}} = 2.0\,\%$ and $E_{\{e,p\}} = 6.7\%$. It is noted that as a result of supplying non-zero sample concentration in inlets 3 and 4, the two single bell shapes partially overlap in the central region, leading to the asymmetry of each individual bell profile. Although not shown here, it is conceivable that the slopes, widths, and position of the constituent bell shape can be manipulated using flow rates, flow ratio, and inlet concentration in a similar manner as the single bell-shaped case. For example, we can apply higher flow rates in the two side inlets (inlets 1 and 6) and lower flow rates in the two central inlets (inlets 3 and 4), *i.e.*, varying the flow ratio, to shift the peaks of the two constituent bell shapes closer to each other.

The concentration profiles selected from model-based design are also compared against the experimental results for model verification. Good agreement is found over the entire channel width, with a relative error of $E_{\{d,e\}} = 7\%$. In addition to flow disturbances as discussed above, the issue of pump mismatch also contributes to experimental error in this case. Here, due to the unavailability of three identical syringe pumps, pumps of different models (characterized by different technical specifications and accuracy levels) were used for double-shaped profile generation. Specifically, the syringe pump used to inject samples to inlets 3 and 4 was different from the other two, which led to larger discrepancies in the central region of the profile, as seen in Fig. 7b.

6. Conclusion

A novel method of generating complex concentration profiles has been presented, which utilizes partial diffusive mixing in multi-stream laminar flow in microfluidic networks. The underlying principle is to combine simple constituent concentration profiles to construct composite profiles with a higher level of complexity. To assist the device design, an iterative algorithm has been developed to integrate previous CGG models as a simulation engine. The iterative process not only captures the overall effects of device geometry, sample properties, and operating protocols on sample transport, but also allows identification of the optimal design parameters. Hence, it enables rapid, effective, and reliable virtual prototyping of CGG for lab-on-a-chip applications.

The iterative design approach is then exploited to devise practically relevant CGG networks that are able to generate user-prescribed concentration profiles. CGG microchips are fabricated using soft lithography and experimentally characterized using the parameters selected from design process. The experimental results successfully demonstrate the generation of a variety of concentration profiles *via* partial mixing and provide several key insights:

1. The qualitative shape of concentration profiles is dictated by the CGG topology. Specifically, simple linear and bell-shaped profiles are obtained from Y- or ψ-shaped mixers, respectively.

Microfluidic networks that laterally line up multiple Y- or ψ-shaped mixers are capable of producing sawtooth- or double/multiple bell-shaped concentration profiles.

2. The details in the concentration profile can be tuned with geometrical and operating parameters. For example, small flow rates (or equivalently, long microchannels) promote sample diffusive mixing; leading to mild, smooth gradients as shown in Fig. 5. Control of flow ratios is effective in terms of modulating the width of certain portions of the profile (Fig. 5b). In addition, given fixed CGG network dimensions, sample concentrations at the reservoirs serve as a practical means for gradient modulation as shown in Fig. 6.

3. Profiles from design and experiments in general show good agreement with the prescribed ones, while appreciable discrepancies caused by the profile bending at the sidewalls and interface region have been observed for the linear and sawtooth cases due to the impermeability conditions therein. Note that such effects are also typically present in complete mixing-based gradient generation approaches[14] with the exception of heavily stacked networks containing a large number of branches,[11] which unfortunately occupy large footprint and are prone to leakage and clogging.

4. Excellent agreement between the experimental data and design profile has been observed in all cases with relative errors less than 10%, which substantiates the accuracy of our previously developed CGG models.

Acknowledgements

We gratefully acknowledge financial support from DARPA and Air Force Research Laboratory, Air Force Material Command, USAF, under grant number F30602-01-2-0587, and from the NSF ITR program under award number CCR-0325344.

References

1 S. J. Wang, W. Saadi, F. Lin, C. M. C. Nguyen and N. L. Jeon, Differential effects of EGF gradient profiles on MDA-MB-231 breast cancer cell chemotaxis, *Experimental Cell Research*, 2004, **300**, 180–189.
2 N. L. Jeon, H. Baskaran, S. K. W. Dertinger, G. M. Whitesides, L. Van de Water and M. Toner, Neutrophil chemotaxis in linear and complex gradients of interleukin-8 formed in a microfabricated device, *Nature Biotechnology*, 2002, **20**, 826–830.
3 X. Y. Jiang, J. M. K. Ng, A. D. Stroock, S. K. W. Dertinger and G. M. Whitesides, A miniaturized, parallel, serially diluted immunoassay for analyzing multiple antigens, *Journal of the American Chemical Society*, 2003, **125**, 5294–5295.
4 P. J. A. Kenis, R. F. Ismagilov, S. Takayama, G. M. Whitesides, S. L. Li and H. S. White, Fabrication inside microchannels using fluid flow, *Accounts of Chemical Research*, 2000, **33**, 841–847.
5 X. Y. Jiang, Q. B. Xu, S. K. W. Dertinger, A. D. Stroock, T. M. Fu and G. M. Whitesides, A general method for patterning gradients of biomolecules on surfaces using microfluidic networks, *Analytical Chemistry*, 2005, **77**, 2338–2347.
6 O. D. Weiner, G. Servant, M. D. Welch, T. J. Mitchison, J. W. Sedat and H. R. Bourne, Spatial control of actin polymerization during neutrophil chemotaxis, *Nature Cell Biology*, 1999, **1**, 75–81.
7 P. C. Wilkinson and J. M. Lackie, The Influence of Contact Guidance on Chemotaxis of Human Neutrophil Leukocytes, *Experimental Cell Research*, 1983, **145**, 255–264.
8 S. Boyden, Chemotactic Effect of Mixtures of Antibody and Antigen on Polymorphonuclear Leucocytes, *Journal of Experimental Medicine*, 1962, **115**, 453.
9 D. Zicha, G. A. Dunn and A. F. Brown, A New Direct-Viewing Chemotaxis Chamber, *Journal of Cell Science*, 1991, **99**, 769–775.
10 S. H. Zigmond, Ability of Polymorphonuclear Leukocytes to Orient in Gradients of Chemotactic Factors, *Journal of Cell Biology*, 1977, **75**, 606–616.
11 S. K. W. Dertinger, D. T. Chiu, N. L. Jeon and G. M. Whitesides, Generation of gradients having complex shapes using microfluidic networks, *Analytical Chemistry*, 2001, **73**, 1240–1246.
12 C. Neumann and S. Cohen, Morphogens and pattern formation, *Bioessays*, 1997, **19**, 721–729.
13 F. Lin, W. Saadi, S. W. Rhee, S. J. Wang, S. Mittal and N. L. Jeon, Generation of dynamic temporal and spatial concentration gradients using microfluidic devices, *Lab on a Chip*, 2004, **4**, 164–167.
14 G. M. Walker, J. Q. Sai, A. Richmond, M. Stremler, C. Y. Chung and J. P. Wikswo, Effects of flow and diffusion on chemotaxis studies in a microfabricated gradient generator, *Lab on a Chip*, 2005, **5**, 611–618.
15 B. R. Gorman and J. P. Wikswo, Characterization of transport in microfluidic gradient generators, *Microfluidics and Nanofluidics*, 2008, **4**, 273–285.
16 Y. Wang, T. Mukherjee and Q. Lin, Systematic modeling of microfluidic concentration gradient generators, *Journal of Micromechanics and Microengineering*, 2006, **16**, 2128–2137.
17 K. Campbell and A. Groisman, Generation of complex concentration profiles in microchannels in a logarithmically small number of steps, *Lab on a Chip*, 2007, **7**, 264–272.
18 M. A. Holden, S. Kumar, E. T. Castellana, A. Beskok and P. S. Cremer, Generating fixed concentration arrays in a microfluidic device, *Sensors and Actuators B-Chemical*, 2003, **92**, 199–207.
19 G. M. Walker, M. S. Ozers and D. J. Beebe, Cell infection within a microfluidic device using virus gradients, *Sensors and Actuators B-Chemical*, 2004, **98**, 347–355.
20 F. M. White, *Viscous fluid flow*, 2nd ed. New York: McGraw-Hill, 1991.
21 J. S. H. Lee, Y. D. Hu and D. Q. Li, Electrokinetic concentration gradient generation using a converging-diverging microchannel, *Analytica Chimica Acta*, 2005, **543**, 99–108.

